Received: 29 October 2018 | Revised: 29 April 2019 | Accepted: 15 May 2019

DOI: 10.1111/jace.16593

ORIGINAL ARTICLE

Journal of the American Ceramic Society

Setting behavior and bioactivity assessment of calcium carbonate cements

Jesús Rodríguez-Sánchez[1] | **Barbara Myszka**[2] | **Aldo Roberto Boccaccini**[2] | **Dag Kristian Dysthe**[1]

[1]Physics of Geological Processes, Department of Physics, NJORD Centre, University of Oslo, Oslo, Norway

[2]Institute of Biomaterials, University of Erlangen-Nuremberg, Erlangen, Germany

Correspondence
Jesús Rodríguez-Sánchez, Physics of Geological Processes, Department of Physics, NJORD Centre, University of Oslo, PO Box 1048 Blindern, Oslo, Norway.
Email: j.r.sanchez@fys.uio.no

Funding information
European Union Horizon 2020 research and innovation program, Marie Skłodowska-Curie, Grant/Award Number: 642976-NanoHeal Project

Abstract

Calcium carbonate cements have emerged in the last few years as an attractive candidate for biomedical applications. They can be easily prepared by mixing water with two metastable calcium carbonate phases—amorphous calcium carbonate (ACC) and vaterite—which (re)crystallize into calcite during setting reaction. The transformation kinetics (and therefore the final surface cement composition) strongly depends on the initial mixture design and is controlled by the dissolution of ACC, whereas calcite nucleation typically controls their recrystallization in fluid batch experiments. Novel compositions are presented in this paper by incorporating organic molecules as a proxy to test their capability to carry on other biomolecules like proteins or antibiotics. The hardened samples are microporous and show excellent bioactivity rates, although their mechanical properties still remain poor. However, this would not be a handicap for in-vivo applications such as bone filling, especially in low mechanical stress locations.

KEYWORDS

(re)crystallization kinetics, apatite-like precipitation, bioactivity, $CaCO_3$ cements, compressive strength

1 | INTRODUCTION

Biomedical ceramics and cements were the first synthetic approaches employed by orthopedics and surgeons to overcome the inherent difficulties associated with natural bone-substitute materials (viral and/or bacterial contamination risks, biological variability or difficulty of supply). More specifically, calcium phosphate cements (CPCs) were the most used and attractive alternatives as a result of their excellent biocompatibility and bioactive properties.[1,2] However, the limited solubility of their main constituent phase (apatite) still represents their leading drawback and in consequence, several CPCs containing more soluble mineral compounds (like calcium sulfate or calcium carbonate, for example[3–5]) were developed to improve their biological resorption rate and subsequent bone formation. Some authors went beyond that idea and proposed cement compositions entirely made of calcium carbonate ($CaCO_3$),[6–8] opening new possibilities since they exhibit not only higher solubility but larger porosity and faster resorption rates among many other advantages.

$CaCO_3$ is a simple compound and one of the most abundant minerals throughout nature. It exists in six different polymorphic phases, which listed from the most to the least thermodynamically stable are: three different anhydrous crystalline phases (calcite, aragonite, and vaterite), two hydrated phases (ikaite and monohydrocalcite), and one amorphous calcium carbonate (ACC) phase. The feasibility of sintering cements entirely made of $CaCO_3$ from those phases

was already demonstrated by Combes et al.[7] The authors stated that it is necessary to prepare biphasic mixtures of calcium carbonate powders comprising metastable phases. One of those should be the highly reactive ACC phase while the other should be one of the metastable crystalline phases, that is, either vaterite or aragonite, to serve as seeds and orient the (re)crystallization of the mixture into a more stable calcium carbonate crystalline phase in the presence of small amounts of water. Nevertheless, a better understanding of this (re) crystallization process is still necessary to optimize these materials since the adequate tuning of the cement composition is crucial to achieve a satisfactory clinical use.

Cements, unlike sintered and natural materials can be easily associated with active biological molecules like proteins or antibiotics.[9,10] However, there is still a lack of understanding about the interactions between organic materials and inorganic cements. For instance, polysaccharides, fatty acids (olive oil), and Nopal juice (a plant extract) have been used in traditional lime mortars to improve some of their properties[11] but in most cases they displayed a negligible impact on the mechanical strength.[12] Nevertheless, recent research has shown that the presence of organic molecules in chalk (a carbonate sedimentary rock) is key to understand its strength on geological time scales.[13] Chalk consists of tiny calcium carbonate crystals (in the form of calcite) that are intrinsically very reactive. If these crystals could recrystallize, chalk would have a very high creep rate under its own load. However, the recrystallization is passivated by the presence of organic molecules. Thus, when a crack appears, the crack surfaces consist of fresh unpassivated calcite that can react to heal the crack. Consequently, the presence of organic additives within cement microstructures may open new possibilities in terms of enhanced mechanical properties and endowment of self-healing properties that will be of great interest, especially for biomedical applications.

In this study we evaluate the reaction kinetics and the composition during setting and hardening of calcium carbonate cements, both in the absence and incorporating octanoic acid (OA) as a proxy to test their capability to carry on biomolecules like proteins or antibiotics and/or to endow them with self-healing properties. Moreover, we assess their bone bioactivity by checking the ability of apatite-like compounds to form on their surface after immersion in simulated body fluid (SBF) as a common practice in the field of bioactive materials.[14–16] The study covers several immersion periods after which both their mechanical properties and degree of apatite precipitation are evaluated.

2 | MATERIALS AND METHODS

2.1 | Preparation of $CaCO_3$ powders

The preparation of $CaCO_3$ cements requires the synthesis of different calcium carbonate polymorphs in order to design the initial cement mixture.[7] Accordingly, both ACC and vaterite phases were prepared as described on.[17] Briefly, they were precipitated by mixing calcium chloride ($CaCl_2{\cdot}6H_2O$, Sigma Aldrich) and sodium carbonate (Na_2CO_3, Sigma Aldrich) equimolar (0.5 mol/L) solutions, prepared with ultrapure Milli-Q water (18.2 MΩ cm), at room temperature using a magnetic stirrer set at 400 rpm. Following Ogino et al[18] we used reaction time 10 seconds for ACC and 30 minutes for vaterite. To wash off any dissolved sodium chloride (NaCl), the $CaCO_3$ precipitates were rinsed with deionized water and ethanol, using a filtering kit and 0.5 μm pore-size filter papers (Millipore, USA). Subsequently, the $CaCO_3$ precipitates were flushed with liquid N_2 to stop the recrystallization of these metastable phases. The frozen precipitates were lyophilized (Alpha 1-4 LD plus, Martin Christ, Germany) for 48 hours at 0.05 mbars and −50°C and stored in a freezer (−22°C) with additional silica powder bags to keep them as dry as possible[19] prior to cement manufacturing.

The precipitates were scanned by X-ray diffraction (XRD) (Bruker D8 Discover X-ray diffractometer) to identify the crystalline phases present using CuK_α radiation (30 mA and 40 kV) and recording 2θ angles from 20° to 50° at a 0.04 s^{-1} sweep rate. Additionally, they were imaged with scanning electron microscopy (SEM) (Hitachi SU5000 Field-Emission; 1 kV acceleration voltage and 3.0 mm working distance).

2.2 | Preparation of $CaCO_3$ cements

Following the method outlined by Combes et al,[7] we synthesized $CaCO_3$ cements with different microstructures by mixing ACC and vaterite powders in different weight ratios (wt%): 1:1, 1:2, and 1:3, respectively, while keeping the liquid to solid ratio (L/S) constant (0.5). Vaterite was selected as our crystalline seed rather than aragonite to simplify the manufacture.

To investigate the influence of organic molecules absorbing on the mineral surfaces within the cement microstructure, we have chosen to study a simple carboxylic acid: octanoic acid. Octanoic acid is a low soluble, eight-carbon saturated fatty acid, which can be found naturally in the milk of various mammals.[20] Due to its length, it has been used as a cross-linker agent in several industries, including coatings and pharmaceutics,[21,22] and consequently it is an interesting candidate to provide self-healing properties to cement pastes. The carboxyl group of octanoic acid is known to absorb on calcite surfaces as monolayers[23] and can either inhibit further calcite growth or enhance it by templating. Two different concentrations, 0.4 and 0.8 vol%, of octanoic acid (OA) (Sigma-Aldrich) were added to the water phase prior to mixing with the solid phase. These values were chosen based on preliminary tests to find the maximum concentration of OA that allows setting of $CaCO_3$ cement pastes (C_{max} = 1.0 vol%).

The notation used hereafter to refer to each composition is the following: 1:1 wt%, 1:2 wt%, and 1:3 wt% for the pure compositions, and 1:2 wt% + 0.4 vol% OA and 1:2 wt% + 0.8 vol% OA for those containing organic molecules. Just after mixing the powders with the liquid phase, the resulting pastes were viscous and easily moldable for several minutes. To ensure reproducibility, sufficient cement quantities were made to perform all analyses on the same sample batch.

2.3 | In-situ time-lapse XRD analysis of cement setting

To quantify the phase transformation kinetics during the setting reaction we have used in-situ x-ray diffraction (XRD) at high temporal resolution (<25 seconds) on the cement pastes. The fresh pastes were molded into sample holders (25 mm discs, 2 mm depth) and firmly tamped immediately after mixing with water.

To identify the crystalline phases present within the precipitates as a function of time, the $CaCO_3$ cement pastes were scanned using a Bruker D8 A25 X-ray diffractometer with MoK_α radiation (48 mA and 48 kV) and recording 2θ angles from 10° to 17° at a sweep rate of 0.035 s^{-1} (See Supplementary Material, SM.1, for further details). The reactions were considered complete when no further changes within the diffraction peak intensities were observed. Further scans were launched after 28 days to discard any possible evolution of the (re)crystallization process with time.

2.4 | Bioactivity assessment in simulated body fluid

2.4.1 | Sample preparation

For the in-vitro studies and accompanying strength testing, wet cement pastes (prepared as described on Section 2.2) were placed in specially designed oedometric presses (hollow cylinders, 12.0 cm in height and 2.0 cm inner diameter) in between two porous, plastic-made, auxiliary discs.[24] The inner walls of the presses were coated with Teflon®. A steel spring loaded uniaxially the assembly at about ~0.15 MPa. Thereupon, the presses were placed inside an oven at physiological temperature (37°C) for setting and hardening for the first 24 hours. After that, the specimens were unmolded and left inside the oven for final drying. This process was followed by means of their weight evolution using digital scales (Sartorious Lab Instruments, Germany, accuracy = 0.1 mg). After 7 days the weight of the samples reached a plateau value and they were cut into smaller cylinders using a metallic saw and polishing paper (silicon carbide P80D) brought to 1.00 ± 0.02 cm in height and 0.50 ± 0.02 cm in diameter. The final dimensions of the specimens were measured using a caliper and used to determine their apparent density, ρ_a.

2.4.2 | In-vitro study with simulated body fluid

Following Kokubo et al,[14] an acellular solution with an ionic composition similar to that of human plasma, known as simulated body fluid (SBF), was prepared for the in-vitro study by dissolving the amounts of reagent chemicals into distilled water (in order): NaCl (137.4 mmol/L), $NaHCO_3$ (4.225 mmol/L), KCl (3.018 mmol/L), $K_2HPO_4{\cdot}3H_2O$ (1.012 mmol/L), $MgCl_2{\cdot}6H_2O$ (1.529 mmol/L), $CaCl_2{\cdot}2H_2O$ (2.631 mmol/L), and Na_2SO_4 (0.506 mmol/L). The next reagent was only added after the previous one was completely dissolved. Then, the solution pH was adjusted to the physiological value (7.40) by HCl (1.0 mol/L) addition and buffered by tris(hydroxyl-methyl) aminomethane (50.505 mmol/L). The equilibrated mass distribution of the ionic species is included on SM.4.

The small pressed cement cylinders were placed in polyethylene flasks, immersed in 50 mL of SBF and incubated at constant temperature (37°C) and orbital shaking (90 rpm) for different periods of time (1, 3, 7, 14, and 28 days). The SBF solution was refreshed every 3 days. After each immersion period, the pH of the solution was measured and the specimens were rinsed; first with distilled water and then with ethanol to terminate further reactions, followed by a 24 hours drying period under a fume hood. Samples were stored in desiccators until further examination.

The formation of apatite-like crystals on the cements placed in the SBF flask was studied by several analytical techniques. First, the dried solid samples were fixed on a support plate using silver paste in between, and analyzed using a secondary electron microscope (1 kV acceleration voltage and 3.0 mm working distance). Second, scratched powder taken with a spatula from the outermost surface was analyzed with XRD and Fourier transform infrared spectroscopy (FTIR). XRD patterns were collected using CuK_α radiation (30 mA and 40 kV), recording 2θ angles from 20° to 50° at a sweep rate of 0.04 s^{-1} and combined with the software Diffrac.EVA (Bruker AXS, USA) for crystalline phase identification. FTIR spectra were recorded using an attenuated total reflection (ATR) cell, in the transmittance mode and within the wavenumber interval 400-4000 cm^{-1}. The analysis was performed in triplicate over newly synthesized samples while unsoaked samples of each composition were used as controls.

2.4.3 | Compressive strength

The compressive strength of the cement cylinders used for the in-vitro bioactivity assessment was tested before and after each immersion period using a DEBEN CT5000 (UK) tensile/compression stage (5000 N load cell, 0.01 N resolution), at a crosshead speed of 0.2 mm/min, corresponding

to strain rates of 10^{-3} s^{-1}. From the recorded data (applied force and sample elongation), a stress–strain curve was constructed for each test. The uniaxial compressive strength (UCS) was computed on the basics of the maximum force applied at failure and the nominal cross-sectional area of each specimen using an in-house developed scrip in Matlab®.[24] Three samples of each composition were tested to ensure repeatability.

3 | RESULTS AND DISCUSSION

3.1 | Characterization of the starting materials

As shown in Ref.[17] ACC precipitates consist of equidimensional spherical nanoparticles (<50 nm in diameter) accompanied by rhombohedral crystals of about 50-100 nm, which were confirmed to be calcite by XRD analysis. Vaterite precipitates consist of spherical grains of 4-5 μm in diameter also accompanied by calcite rhombohedral grains (4-5 μm). An analysis of the XRD patterns using the software Diffrac. Suite TOPAS (Bruker AXS, USA) derived a composition of 86% ACC and 14% calcite for ACC precipitates while a 93% vaterite and 7% calcite for vaterite precipitates.

3.2 | (Re)crystallization analysis and final composition of $CaCO_3$ cements

Cement compositions and transformation kinetics of different $CaCO_3$ phases involved during setting and hardening processes are investigated by in-situ time-resolved XRD. Figure 1 includes an example 3D plot of the XRD patterns obtained from the cement composition 1:1 wt%. At the base of each pattern there is a slightly curved baseline, resulting from the combined scattering of the poorly ordered ACC and the aqueous solution.[25] Moreover, immediately upon mixing of the starting reagents with water, the distinctive diffraction peaks of both vaterite and calcite are observed, with a more prominent calcite peak.

With ongoing transformation, the broad hump and the tandem vaterite peaks start to break down, while the calcite peaks become more prominent. It is important to highlight that the rates at which these phases dissolve and/or (re)crystallize do not only vary with time but also are concentration-dependent, so their values are different for each of the studied cement compositions.

3.2.1 | The effect of starting composition

Figure 2 includes the calculated molar fractions, X_i, of the three calcium carbonate polymorphs (ACC, vaterite, and calcite) that coexist during the setting reaction for three different $CaCO_3$ pure compositions (1:1, 1:2 and 1:3 wt% ACC:V). It shows visually how the two starting phases—ACC and vaterite—are dissolving while the third one—calcite—is growing at the expense of the other two. The results show that the reaction rate, and thus the crystallization process, depends on the initial weight ratio between ACC and vaterite powders, as does the total duration of reaction. Moreover, it seems that only the 1:1 wt% paste is able to complete the transformation. After 10 hours of reaction, the remaining amount of vaterite for this composition is almost undetectable (2 ± 1%) and the specimen is entirely made of calcite (98 ± 2%). Thus, both setting and hardening processes are fast enough to complete the (re)crystallization of the initial admixture into the most stable $CaCO_3$ phase before drying.

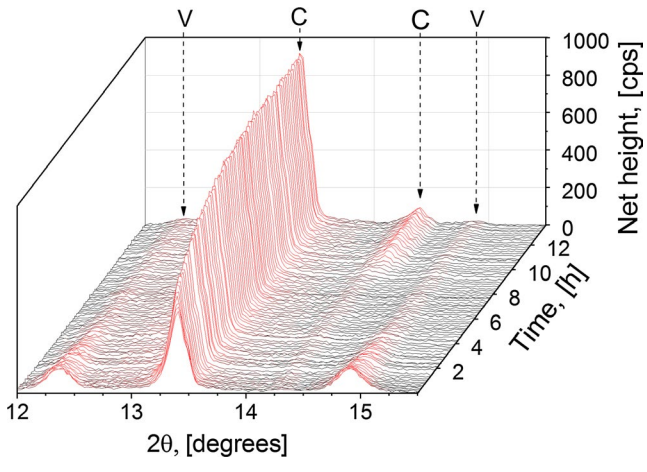

FIGURE 1 3D plot of time-lapse XRD patterns obtained from the cement composition 1:1 wt% showing the evolution of the solid phases ACC, vaterite, and calcite. Colored peaks just to guide the eye

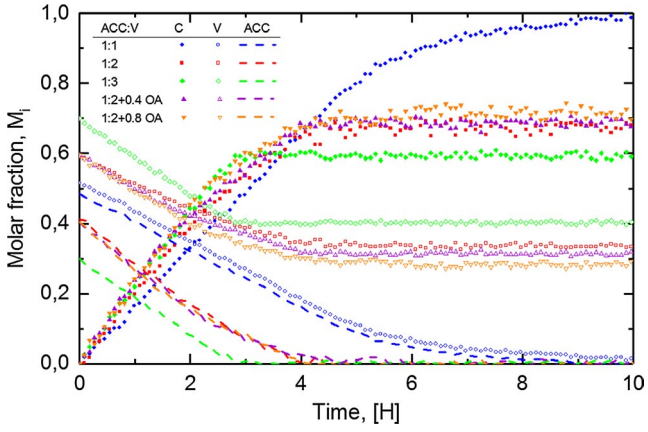

FIGURE 2 Calcite, vaterite, and ACC mole fractions, X_i, evolution with time for three different pure $CaCO_3$ cement compositions (1:1, 1:2, and 1:3 wt% ACC:V), and two $CaCO_3$ cement compositions containing organics. Solid symbols represent calcite while empty symbols and dashed lines stand for vaterite and ACC, respectively

TABLE 1 Transformation kinetics during setting and hardening and final composition of several calcium carbonate cement pastes measured from in-situ time-lapse XRD scans

Sample	Total reaction time (h)	Final composition (%)		Time constant, τ (h) dissolution model	Final density, σ (g/cm^3)
		Calcite	Vaterite		
1:1 wt%	10.00	98 ± 2	2 ± 1	12	1.11 ± 0.01
1:2 wt%	4.50	66 ± 2	33 ± 1	7	1.09 ± 0.02
1:3 wt%	3.00	59 ± 2	40 ± 1	5	1.08 ± 0.02
1:2 wt% + 0.4 vol% OA	4.60	68 ± 2	31 ± 1	7	1.16 ± 0.08
1:2 wt% + 0.8 vol% OA	4.90	70 ± 2	29 ± 1	7	1.20 ± 0.05

The 1:2 wt% paste transforms more rapidly than the previous composition, following a linear evolution up to 3 hours of reaction when it starts to deviate. After ~4.5 hours no more changes among crystalline diffraction intensities are detected and the reaction is stopped. Nevertheless, the results show that the drying process does not allow a complete transformation of the initial phases since the set sample contains 66 ± 2% calcite and 33 ± 1% untransformed vaterite.

An even faster crystallization mechanism, as well as earlier termination, can be recognized for the 1:3 wt% composition. Calcite transformation kinetics also follows a linear evolution and after 3 hours of reaction, a sudden arrest makes the set sample to be composed by 59 ± 2% calcite and 40 ± 1% untransformed vaterite. The complete arrest of transformation of vaterite into calcite coincides in time with the completion of transformation of ACC. The coupling of the transformation kinetic timescales of vaterite and ACC in these experiments is in contrast to the decoupled timescales of transformation in previous experiments, where the samples were plastic covered to avoid evaporation.[17] However, during the experiments here presented there was water evaporation to allow a more natural coupling of setting and drying. The fact that when there is no more ACC all transformation stops suggests that water is mainly trapped in the very small pores between the tiny ACC grains, whereas the coarser vaterite grains dry out quickly and are only supplied with water for transformation by the adjacent ACC. All these results are summarized in Table 1.

In order to model this behavior, we follow[17] and describe the crystal dissolution rate, r (See SM.2, for further details).

Previously,[17] we found that for wet $CaCO_3$ cements the transformation mechanism was limited by the dissolution of vaterite and not by the available surface area of calcite as has been reported for batch experiments.[18,26] In the present case of drying and recrystallizing cement, we employ an ACC dissolution model which analyzes the evolution of the mass, m, of ACC. The theoretical interpretation coming out from this model is included on Figure 3 (solid line) along with the experimental data measured herein for the ACC phase from different cement pastes (ACC:V ratios). The obtained time

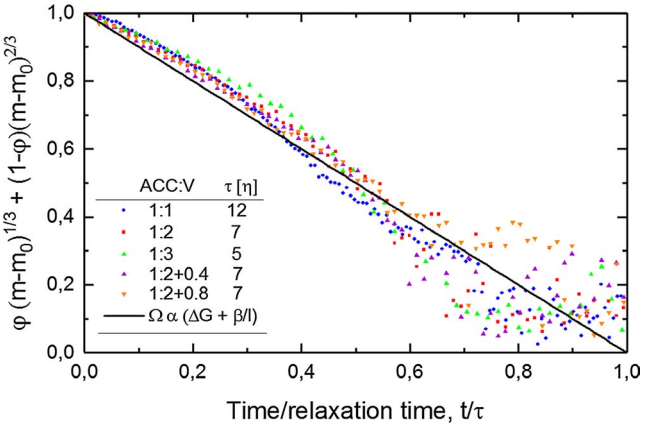

FIGURE 3 Normalized ACC mass evolution with time for three different pure $CaCO_3$ cement compositions (1:1, 1:2, and 1:3 ACC:V wt%) considering the supersaturation, Ω, proportional to the Gibbs free energy of the system ΔG. The solid line shows the outcome of the ACC dissolution model (Equation SM.5)

constant values, τ, are $\tau_{ACC:V\ 1:1} = 12$ hours, $\tau_{ACC:V\ 1:2} = 7$ hours, and $\tau_{ACC:V\ 1:3} = 5$ hours. As for our previous study, there is a good agreement between the model and the data, which supports that the transformation of ACC to calcite within a cement paste system is limited by the dissolution of ACC, even under different setting conditions which do not allow a complete phase (re)crystallization of the initial reagents within the paste. It is clear that the time constant $\tau \propto \frac{1}{K\Omega}\left(\frac{m_{V,0}}{N}\right)^{1/3}$ changes for each of the initial cement mixtures, increasing with the initial ACC content.

During the transformation, the liquid phase of the cement paste remains supersaturated with respect to calcite driving the precipitation of this phase. The resulting fine calcite crystallites begin to form an interconnected microstructure with particular pore structure and geometrical distribution. We suggest that subsequent crystal growth causes further hardening and strengthening of the cement matrix toward an overall mechanical resistance.

XRD scans after 28 days discarded further changes within the cement compositions listed on Table 1.

3.2.2 | The (lack of) effect of organic molecules

Figure 2 also shows the calculated molar fractions, X_i, of the three calcium carbonate polymorphs (ACC, vaterite and calcite) that coexist during the setting reaction for two $CaCO_3$ pastes with imbibed organic molecules. The 1:2 wt%+0.4 vol% OA specimen transforms linearly into calcite as without OA. After 4 hours and 36 minutes, the reaction is completed and the set sample contains 68 ± 2% calcite and 31 ± 1% untransformed vaterite. For the 1:2 wt%+0.8 vol% OA paste, the reaction is over after 4 hours and 54 minutes, leading to slightly greater final calcite content (70 ± 2%) and slightly lower untransformed vaterite amount (29 ± 1%). Moreover, XRD patterns remain nearly unchanged after 28 days as for the pure samples. Hence, a delayed effect of OA molecules among the $CaCO_3$ phase transformation mechanism is discarded.

The results show that the presence of OA molecules does not significantly modify the reaction rate nor the final phase composition when compared with their reference microstructure. Slightly longer reaction times lead to some extend higher calcite and consequently, somewhat lower vaterite amounts (Table 1). Moreover, the corresponding time constants, τ, obtained from the ACC dissolution model are the same as those obtained for the 1:2 wt% composition ($\tau_{ACC:V\ 1:2 + 0.4\ OA} = 7$ hours and $\tau_{ACC:V\ 1:2 + 0.8\ OA} = 7$ hours).

Within the experimental uncertainty, the results show that there is no effect of OA on calcium carbonate (re)crystallization. This signifies that OA does not impede calcite crystallization enough to become the rate limiting process. We may also conclude that OA does not change the dissolution rate of ACC or vaterite (within the range studied). Similar results were reported for carbonic anhydrase enzyme on lime mortars carbonation process.[27] Thus, these results are encouraging with respect to the inclusion of other biomolecules like proteins or antibiotics (within similar concentrations) which may enhance other properties of the cements (like protein adhesion, bactericidal effect, drug release, etc.) without modifying the crystallization pathway of the pastes since that is mainly determined by the starting mixture design.

3.3 | $CaCO_3$ cements bioactivity

3.3.1 | Scanning electron microscopy (SEM) analysis

Figure 4 includes an example set of surface SEM micrographs obtained for the 1:1 wt% composition (A) before immersion and after soaking in SBF for (D) 7 days, (E) 14 days, and (F) 28 days (See Figure SM.2 for (B) 1 day and (C) 3 days). The images obtained for all the other compositions are similar, including those containing organic molecules.

Figure 4A shows a microporous entangled network of small (>5 μm) rhombohedral calcite crystals. No changes are observed in the cement surface (Figure SM.2B, 1 day and C, 3 days) until 7 days of immersion (Figure 4D) when the first apatite-like crystals (~2 μm) are detected. They are randomly distributed along the surface regardless of any topographical features. One extra week of immersion (Figure 4E) results not only on double-sized (~5 μm) apatite-like crystals but also in a partly covered cement surface since those crystals start to merge and to form a smooth layer. Upon immersion for 28 days (Figure 4F), almost the entire cement surface is covered by a uniform apatite-like layer (identified by its crystal habit). Once again the crystal size has roughly doubled indicating an approximately constant growth rate of 0.3 μm/day.

The appearance of well defined, isolated apatite spheres indicates that there is a significant nucleation barrier to the apatite formation. Two different mechanisms may be suggested to explain the formation of apatites in SBF solutions. The former considers that the SBF itself is supersaturated with respect to most calcium phosphates (except brushite ($CaHPO_4{:}2H_2O$) and monetite ($CaHPO_4$), See SM.4 and Ref. [28]) and those may precipitate. However the concentration of Ca^{+2} and PO_4^{-3} ions available for precipitation of calcium phosphates in 50 mL of SBF solution is very small (See SM.4, Table SM.2). On the other hand, the latter suggests that the process requires the dissolution of calcite from the sample tested to supply Ca^{2+} ions, despite the very low solubility of calcite (0.013 g/L at 25°C[29]). Nevertheless, the actual Ca/P ratio of the SBF solution is around 2.6 and even if we accept that some carbonate ions are recycled in the apatite formed, its Ca/P ratio may reach 1.8-2.0 at most, leaving free calcium in the solution. Thus, the successive soaking volume of SBF in our experiments seems to be insufficient on PO_4^{-3} ions to really change the bulk composition of the cement and this suggests that the former mechanism might be the active one despite of the low ionic concentrations. Moreover, the final layer of apatite crystals was too thin to be correctly analyzed using energy dispersive x-rays (EDS), allowing a high contribution of Ca^{+2} counts coming from the bulk cement.

It is important to mention that drying kinetics of $CaCO_3$ samples used to perform this study are most likely dissimilar from those used to follow their composition during setting due to their geometrical differences. Regardless of the initial mixture design, this fact will lead to gradual compositions from the core of the samples toward their surface, but the amounts included on Table 1 can, at least, be considered as representative of their surface distribution as XRD results confirmed (See Section 3.3.3). Under this base, SEM results suggest that those constitutional differences do not alter the bioactive properties of $CaCO_3$ cements.

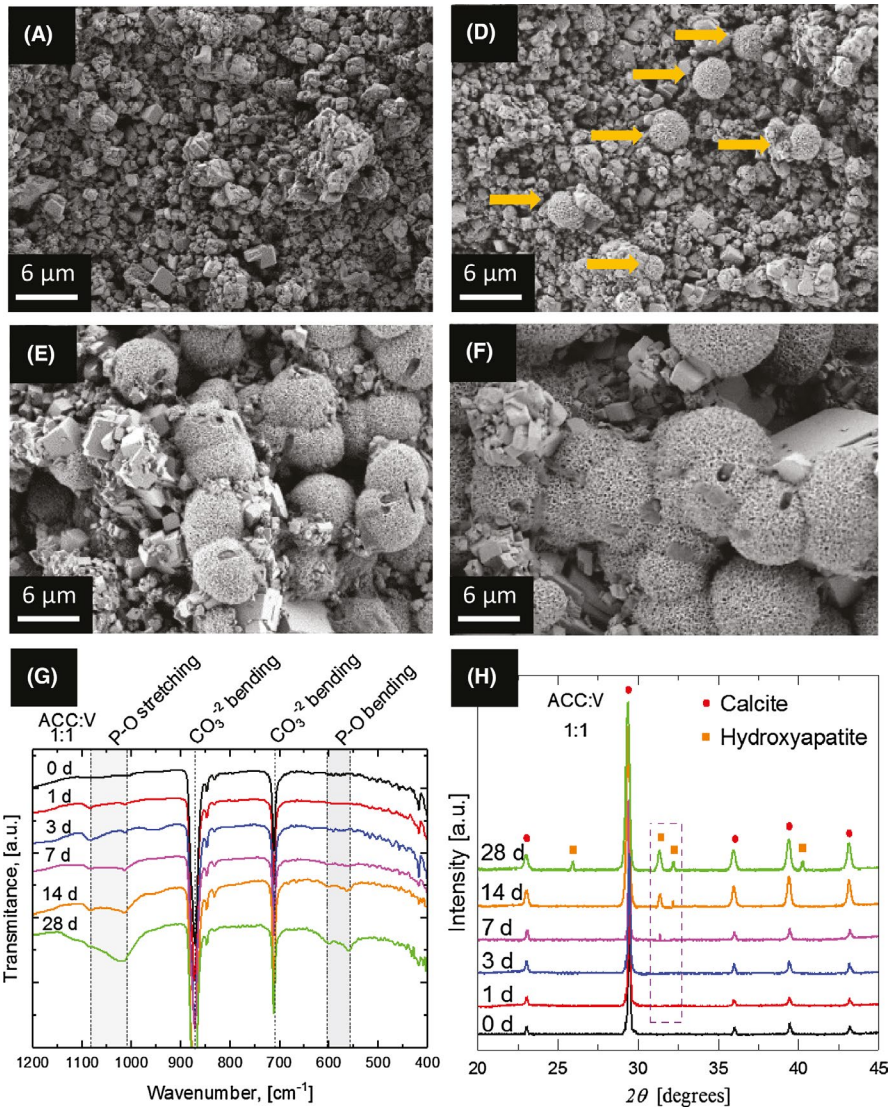

FIGURE 4 SEM micrographs obtained for the 1:1 wt% composition (A) before immersion in SBF and after soaked in SBF for, (D) 7 d, (E) 14 d, and (F) 28 d. The arrows show the first apatite-like structures detected, (G) FTIR spectra, and (H) XRD patterns of the $CaCO_3$ 1:1 wt% composition after immersion in SBF for 0, 1, 3, 7, 14, and 28 days

3.3.2 | Fast transform infrared spectroscopy (FTIR) analysis

The FTIR spectra of the $CaCO_3$ 1:1 wt% specimen immersed in SBF for 0, 1, 3, 7, 14, and 28 days are summarized in Figure 4G. The intense contribution at the CO_3^{-2} out-of-plane and asymmetric bending bands located at 880 and 720 cm^{-1}, respectively, is unsurprising since the cement is fully made of $CaCO_3$.[30,31] Moreover, all spectra capture signal from P–O bands, which are linked to apatite (PO_4^{-3} asymmetric stretching and bending modes located at 1010-1090 cm^{-1} [31,32] and 604-560 cm^{-1},[33] respectively). Even though their intensity increases with the immersion time, only lines measured on absorbance mode are proportional to the concentration but their presence provides further evidence for the formation of apatite-like structures and as such confirms the SEM observations.

Overall, the results obtained for the other cement compositions are similar to the ones included here, in agreement with SEM observations and comments.

3.3.3 | X-ray diffraction (XRD) analysis

For the $CaCO_3$ 1:1 wt% composition, the XRD patterns (Figure 4H) obtained upon soaking in SBF for 0, 1, 3, 7, 14, and 28 days, indicate that calcite is the final surface phase for this cement composition and that apatite-like crystals are of detectable size after 7 days of immersion. It is worth mentioning that the intensity recorded by XRD strongly depends on the degree of crystallinity of the scanned phases whereas vibrational spectroscopies (FTIR) are less sensitive to this parameter. This circumstance may explain why FTIR peaks (previous section) are more intense than the XDR peaks included on Figure 4H. However, looking closely there are two weak peaks (located at 32° and 33°) associated with apatite which increase in intensity with the immersion time (rectangular area in Figure 4H). Since no other intermediate crystalline phases are present, we can confirm that the reaction to form apatite-like structures was complete.

XRD patterns of powdered samples scratched from unsoaked specimens confirmed that the values included on Table 1 can be representative of the surface composition of larger specimens, despite of the dissimilar drying kinetics.

Regarding the nucleation and growth of apatite-like structures, the results obtained for the other compositions are analogous, confirming that the bioactive properties do not depend on the cement surface composition, that is,. the kinetics for nucleation and growth of apatite-like crystals over their surfaces are identical for all of them. During the initial stage of apatite growth, the mass of precipitate is nucleation-controlled whereas when the entire surface is covered after approximately a month, the growth is reaction-controlled.

The crystalline apatite-like nucleation can be taken as a proxy for the bioactive properties of the herein investigated $CaCO_3$ cement compositions at in vivo conditions. In addition, the development of an apatite-like layer upon 28 days of immersion is expected to enhance the cement bone-bonding aptitude since it plays a crucial role at the cement-bone interface as it has been showed for other cementitious materials.[34] It is also noteworthy to mention that no changes in pH (7.40 ± 0.10) are observed in the SBF solutions after the tests and consequently none of the cements are neither highly acidic nor basic compounds.

In addition to the bone-bonding ability, it is generally accepted that micrometer surface roughness not only facilitates the degradation of the materials leading to higher bioactivity rates[35,36] but enhance bone formation, protein adsorption, and cell proliferation.[37,38] Given our SEM observations (Figure 4A-F), the cements herein prepared are expected to be excellent bonding surfaces.

The results also show that octanoic acid does not compromise the bioactive properties of the cement pastes (within the concentration range studied). Consequently, it might contribute to enhance their overall performance. Further studies, however, will be necessary to confirm this approach extending the analysis to other molecules with diverse carbon-chain lengths, concentrations, and/or pH.

3.3.4 | Effect of SBF immersion on uniaxial compressive strength (UCS)

The UCS of all $CaCO_3$ cements herein studied after immersion in SBF for 0 (also referred as unsoaked samples), 1, 3, 7, 14, and 28 days is included in Figure 5. Among pure unsoaked samples, the 1:3 wt% composition shows the highest UCS, followed by the 1:2 wt% and the 1:1 wt%, subsequently. Regarding the two compositions with imbibed organics, 1:2 wt% + 0.4 vol% OA and 1:2 wt% + 0.8 vol% OA, their compressive strength is about 30% lower than that of their counterpart without organics (1:2 wt%).

The dissimilar mechanical properties of unsoaked compositions can be due to several reasons. On previous sections

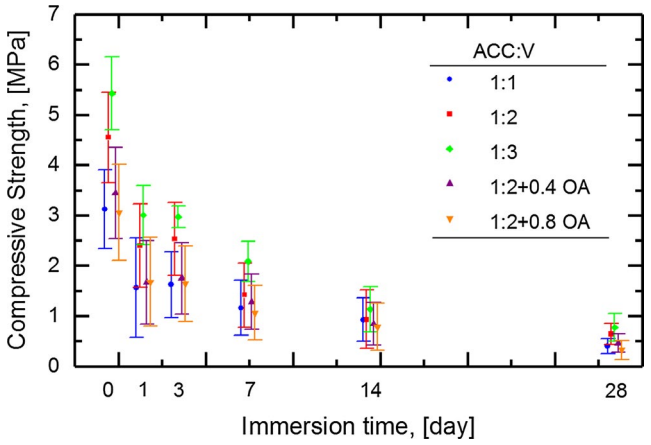

FIGURE 5 Compressive strength of $CaCO_3$ cements before (unsoaked) and after immersion in SBF for 1, 3, 7, 14, and 28 d. Data are presented as mean values ± standard deviation (n = 3)

we suggested that newly formed calcite crystallites may begin to form an interconnected microstructure with particular pore structure and geometrical distribution. Moreover, we suggested that subsequent crystal growth may cause further hardening and strengthening of the cement matrix toward an overall mechanical resistance. Thus, under this hypothesis it seems that the final porosity and the strength of the crystal bridges formed may play the major roles on the mechanical properties of set samples.

The apparent densities, ρ_a, calculated for the 1:1 wt%, 1:2 wt%, and 1:3 wt% set specimens are 1.11 ± 0.01, 1.09 ± 0.02, and 1.08 ± 0.02 g/cm^3, respectively. By comparing these values with the density of bulk calcite ($\rho_{calcite}$ = 2.71 g/cm^3)[3,39] a porosity of about 59%-61% can be estimated for all of them. Furthermore, the apparent densities, ρ_a, calculated for 1:2 wt% + 0.4 vol% OA and 1:2 wt% + 0.8 vol% OA are 1.16 ± 0.08 g/cm^3 and 1.20 ± 0.05 g/cm^3, respectively, despite of the lower weight to volume ratio of octanoic acid (0.91 g/cm^3).[20] Comparing those values with the density of calcite, porosity of about 55%-57% can be estimated. Even though it has been shown that each cement composition has its particular distribution of $CaCO_3$ phases after the setting reaction (at least on their surface), the approximation used here to determine the porosity is fairly accurate since the two most abundant phases within set samples, that is, calcite and vaterite ($\rho_{vaterite}$ = 2.64 g/cm^3)[3,39] have a similar density. Thus, the absence of statistical differences within the porosity suggest that the origin of the dissimilar mechanical properties is more likely to be related with the strength of crystal bridges formed during setting. Indeed, this suggestion is consistent with our previous study of $CaCO_3$ cement strength,[17] where we reported a direct relationship between the (re)crystallization extent and the structural development of $CaCO_3$ cement pastes. Moreover, we predicted better mechanical properties

for ACC:V cement mixtures with a larger proportion of vaterite, and indeed this statement is confirmed here. An analogous situation was found for tricalcium silicate (C_3S) pastes with the same porosity but diverse elastic modulus, *E*, and hardness, *H*, remarking again the importance of the solid phases, their volumetric distribution and the joints strength in controlling the final mechanical properties.[40]

For samples soaked in SBF, the results show that the UCS dramatically drops for all compositions since the first day of immersion, from where it continues decreasing with immersion time but less harmfully. For instance, the UCS of the 1:3 wt% drops by a 45% just after 1 day of immersion while it requires 10 more days soaked to drop another 45%. A tempting reasoning to explain this weakening is the dissolution of calcite although none of the hand specimens showed visual signs of degradation. Nonetheless, calcite dissolution is not feasible since the SBF solution is already saturated with respect to calcite at 37°C according to the SBF composition. However, the formation of calcium phosphates (possibly amorphous) even at the first soaking will considerably deplete the solution in Ca^{+2} and PO_4^{-3} and may induce the dissolution of calcite, but further studies will be necessary to check this approach. Moreover, weakening due to the modification of capillary forces within the cement grains can also be a feasible reasoning as it has been reported previously for other cemented rocks.[41,42]

Greater density and the development of an apatite-like layer are features usually associated with a better mechanical performance.[43,44] However, the results show that the denser compositions here studied, that is, those containing organic molecules, have a lower UCS than their counterpart without organic molecules (1:2 wt% pastes) after all soaking periods. Thus, the presence of organics seems to be detrimental for the mechanical properties of the entangled crystalline network. A possible explanation can be a reduction in the overall joint area within the crystals of the network along with the formation of insoluble salts with calcium or other calcium complexes which will not form strong bonds with the carbonate network. However, further characterization of the interactions mechanisms between calcite and OA will be necessary to identify the actual mechanisms.

Comparing the UCS results with the bioactive rates obtained, the results show that the degradation kinetics of the cements are greater than that of apatite-like nucleation and growth for all compositions and hence, the influence of the apatite-like layer on the mechanical properties is not captured.

To evaluate the potential use of bioactive $CaCO_3$ cements, their strength must be compared with that of human bones. For instance, the average femur bone compressive strength is about 130 MPa,[45] which is 23 times higher than the largest value herein measured. From the previous interpretation, it seems that the packing density of the cement samples, and hence the UCS, can be improved by letting the pastes to set under higher pressures. However, further studies are still necessary to check this approach. Even though the overall compressive strength of $CaCO_3$ cements remains poor, such mechanical properties would not be a handicap for secondary in vivo applications like as bone-filling, especially in low mechanical stress locations since the release of calcium and carbonate ions is believed to enhance the formation of new bone tissues.[7]

4 | CONCLUSIONS

The cementing behavior of biomedical soluble calcium carbonate cements has been evaluated for different paste designs, both in the absence and incorporating octanoic acid as a proxy for organic molecules. Time-revolved in-situ x-ray diffraction results showed that the (re)crystallization kinetics depend on the reagent concentration, producing typical microstructures. All starting compositions lead to microporous samples composed of >59% calcite being the transformation from ACC and vaterite to calcite controlled by the dissolution of ACC. A higher initial vaterite concentration has the dual effect of boosting the reaction rate, as well as an early termination.

The inclusion of organic molecules within the cement microstructures, however, does not generate specific behavior within the concentration range studied, opening the possibility to extend the study to other kind of biomolecules like proteins or antibiotics.

The bioactive properties of $CaCO_3$ cements have been confirmed by apatite-like nucleation after 7 days of immersion in simulated body fluid and the development of a bone-like layer beyond that point, regardless of their surface composition or imbibed organics. This coating is expected to enhance the bone bonding aptitude of these cements. Even though the compressive strength of all $CaCO_3$ cements remained poor, their high solubility, fast setting kinetics and bioactive properties still makes them suitable candidates for in vivo applications such as bone filler, especially in low mechanical stress locations.

ACKNOWLEDGMENTS

This project has received funding from the European Union Horizon 2020 research and innovation program under the Marie Skłodowska-Curie grant agreement no. 642976-NanoHeal Project. J.R.-S. would like to express his thanks to David Wragg (University of Oslo) for his assistance analyzing XRD data, to Francois Renard (University of Oslo) for making possible the compressive strength tests, to Aldo Boccaccini (Friedrich-Alexander Universität Erlangen-Nürnberg) for hosting him at the Institute of Biomaterials and to Anne Pluymakers (University of Oslo) for her comments

on an early version of the manuscript. The authors also acknowledge the comments from two anonymous reviewers.

ORCID

JesúsRodríguez-Sánchez https://orcid.org/0000-0002-5259-4707

AldoRobertoBoccaccini https://orcid.org/0000-0002-7377-2955

Dag Kristian Dysthe https://orcid.org/0000-0001-8336-5061

REFERENCES

1. Wang X, Ye J, Wang Y, Ling C. Self-setting properties of a b-dicalcium silicate Reinforced calcium phosphate cement. J Biomed Mater Res B Appl Biomater. 2007;83(2):340–4.
2. Fernandez E. Encyclopedia of biomedical engineering. NY: John Wiley & Sons Inc, NY, 2006; 1–9 p.
3. Heughebaert J, Nancollas G. Kinetics of crystallization of octacalcium phosphate. J Phys Chem. 1957;;88(12):2478–81.
4. Brecevic L, Nielsen AE. Solubility of amorphous calcium carbonate. J Cryst Growth. 1989;98(3):504–10.
5. Bohner M. New hydraulic cements based on a-tricalcium phosphate- calcium sulfate dihydrate mixtures. Biomaterials. 2004;25(4):741–9.
6. Fontaine M-L, Combes C, Sillam T, Dechambre G, Rey C. New calcium carbonate-based cements for bone reconstruction. Key Eng Mater [Internet]. 2015;284-286:105–8. Available from http://www.scientific.net/KEM.284-286.105.
7. Combes C, Miao B, Bareille R, Rey C. Preparation, physical-chemical characterisation and cytocompatibility of calcium carbonate cements. Biomaterials. 2006;27(9):1945–54.
8. Combes C, Tadier S, Galliard H, Girod-Fullana S, Charvillat C, Rey C, et al. Rheological properties of calcium carbonate self-setting injectable paste. Acta Biomater. 2010;6(3):920–7.
9. Lucas A, Gaudé J, Carel C, Michel JF, Cathelineau G. A synthetic aragonite-based ceramic as a bone graft substitute and substrate for antibiotics. Int J Inorg Mater. 2001;3(1):87–94.
10. Blom EJ, Klein-Nulend J, Wolke JGC, van Waas MaJ, Driessens FCM, Burger EH. Transforming growth factor-beta1 incorporation in a calcium phosphate bone cement: material properties and release characteristics. J Biomed Mater Res. 2002;59(2):265–72.
11. Rodriguez-Navarro C, Ruiz-Agudo E, Burgos-Cara A, Elert K, Hansen EF. Crystallization and colloidal stabilization of $Ca(OH)_2$ in the presence of nopal juice (opuntia ficus indica): implications in architectural heritage conservation. Langmuir. 2017;33(41):10936–50.
12. Ventola L, Vendrell M, Giraldez P, Merino L. Traditional organic additives improve lime mortars: New old materials for restoration and building natural stone fabrics. Constr Build Mater. 2011;25(8):3313–8.
13. Hassenkam T, Johnsson A, Bechgaard K, Stipp SLS. Tracking single coccolith dissolution with picogram resolution and implications for CO_2 sequestration and ocean acidification. Proc Natl Acad Sci. 2011;108(21):8571–6.
14. Kokubo T, Takadama H. How useful is SBF in predicting in vivo bone bioactivity? Biomaterials. 2006;27(15):2907–15.
15. Zhang R, Ma PX. Poly(a-hydroxyl acids)/hydroxyapatite porous composites for bone- tissue engineering. I. Preparation and morphology. J Biomed Mater Res. 1999;44(4):446–55.
16. Hench LL, Andersson O. Bioactive glasses. In: LL Hench, J Wilson, editors. An Introduction to Bioceramics. Florida, FL: World Scientific Publishing Co Pte Ltd, 1993; p. 41–62. https://doi.org/10.1142/2028
17. Rodríguez-Sánchez J, Liberto T, Barentin C, Dysthe DK. Mechanisms of phase transformation and creating mechanical strength in a sustainable calcium carbonate cement. 2018. Preprints. https://doi.org/10.20944/preprints201810.0526.v1
18. Ogino T, Suzuki T, Sawada K. The formation and transformation mechanism of calcium carbonate in water. Geochim Cosmochim Acta. 1987;51(10):2757–67.
19. Konrad F, Gallien F, Gerard DE, Dietzel M. Transformation of amorphous calcium carbonate in air. Cryst Growth Des. 2016;16(11):6310–7.
20. Budavari S. The Merck index: an encyclopedia of chemicals, drugs, and biologicals. Whitehouse Station, NJ: Merck; 1996.
21. Fäcke TRS, Dvorchak M, Feng S.Diethylmalonate blocked I isocyanates as crosslinkers for low temperature cure powder coatings. International Waterborne, High-Solids, and Powder Coatings Symposium.2004.
22. James S. Global automotive coatings market. San Francisco, CA: Grand View Research, Inc.; 2015.
23. Hakim SS, Olsson MHM, Sørensen HO, Bovet N, Bohr J, Feidenhans'l R, et al. Interactions of the calcite 10.4 surface with organic compounds: structure and behaviour at mineral – organic interfaces. Sci Rep. 2017;7(1):7592.
24. Rodríguez-Sánchez J, Zhang Q, Dysthe DK. Microstructure and relative humidity effects on long-term indentation creep properties of calcium carbonate cement. 2018. Preprints. https://doi.org/10.20944/preprints201810.0671.v1
25. Faatz M, Gröhn F, Wegner G. Amorphous calcium carbonate: synthesis and potential intermediate in biomineralization. Adv Mater. 2004;16(12):996–1000.
26. Rodriguez-Blanco JD, Shaw S, Benning LG. The kinetics and mechanisms of amorphous calcium carbonate (ACC) crystallization to calcite, via vaterite. Nanoscale. 2011;3(1):265–71.
27. Cizer Ö, Ruiz-Agudo E, Rodriguez-Navarro C. Kinetic effect of carbonic anhydrase enzyme on the carbonation reaction of lime mortar. Int J Archit Herit. 2018;3058(January):1–11.
28. Habraken W, Habibovic P, Epple M, Bohner M. Calcium phosphates in biomedical applications: materials for the future? Mater Today. Elsevier Ltd. 2016;19(2):69–87.
29. Aylward G, Findlay TSI. Section 3: Inorganic compounds. In: A Blackman, L Gahan, editors. Aylward and Findlay's SI Chemical Data. 7th ed. Milton, Austalia: John Wiley & Sons; 2008.
30. Serra J, Gonzalez P, Liste S, Serra C, Chiussi S, Leon B, et al. FTIR and XPS studies of bioactive silica based glasses. J Non Cryst Solids. 2003;332(1–3):20–7.
31. Pryce RS, Hench LL. Tailoring of bioactive glasses for the release of nitric oxide as an osteogenic stimulus. J Mater Chem. 2004;14(14):2303.
32. Muresan D, Bularda M, Popa C. Structural and biological investigations of phosphate glasses with silver. Rom J Phys. 2004;2006(51):231–7.
33. Gonzalez-Hernandez J, Perez-Robles JF, Ruiz F, Martinez JR. Vidrios SiO_2 nanocompuestos preparados por sol-gel: revisión. Superf y vacio. 2000;11:1–16.

34. Gholami F, Zein SHS, Gerhardt LC, Low KL, Tan SH, McPhail DS, et al. Cytocompatibility, bioactivity and mechanical strength of calcium phosphate cement reinforced with multi-walled carbon nanotubes and bovine serum albumin. Ceram Int. Elsevier. 2013;39(5):4975–83.
35. Li R, Clark AE, Hench LL. An investigation of bioactive glass powders by sol-gel processing. J Appl Biomater. 1991;2(4):231–9.
36. Jones JR. Review of bioactive glass: from Hench to hybrids. Acta Biomater. 2015;23(S):S53–82.
37. Zhang L, Webster TJ. Nanotechnology and nanomaterials: promises for improved tissue regeneration. Nano Today. 2009;4(1):66–80.
38. Lord MS, Foss M, Besenbacher F. Influence of nanoscale surface topography on protein adsorption and cellular response. Nano Today. 2010;5(1):66–78.
39. Schroeder BB, Harris DD, Smith ST, Lignell DO. Theoretical framework for multiple-polymorph particle precipitation in highly supersaturated systems. Cryst Growth Des. 2014;14(4):1756–70.
40. Zhang Q. Creep properties of cementitious materials: effect of water and microstructure. An approach by microindentation. Ecole des Ponts ParisTech. 2014.
41. Lord CJ, Johlman CL, Rhett DW. Is capillary suction a viable cohesive mechanism in chalk ?. Soc Pet Eng. 1998: 479–485.
42. Al-Maamori HMS, El Naggar MH, Micic S. Wetting effects and strength degradation of swelling shale evaluated from multistage triaxial test. Undergr Sp. 2019;4(2):79–97.
43. Rodriguez-Lorenzo LM, Vallet-Reg M, Ferreira JMF, Ginebra MP, Aparicio C, Planell JA. Hydroxyapatite ceramic bodies with tailored mechanical properties for different applications. J Biomed Mater Res. 2002;60(1):159–66.
44. Xu HHK, Quinn JB, Takagi S, Chow LC, Eichmiller FC. Strong and macroporous calcium phosphate cement: Effects of porosity and fiber reinforcement on mechanical properties. J Biomed Mater Res. 2001;57(3):457–66.
45. Havaldar Raviraj, Pilli Sc, Putti Bb. Insights into the effects of tensile and compressive loadings on human femur bone. Adv Biomed Res. 2014;3(1):101

SUPPORTING INFORMATION

Additional supporting information may be found online in the Supporting Information section at the end of the article.

How to cite this article: Rodríguez-Sánchez J, Myszka B, Boccaccini AR, Dysthe DK. Setting behavior and bioactivity assessment of calcium carbonate cements. *J Am Ceram Soc*. 2019;00:1–11. https://doi.org/10.1111/jace.16593